

B&P # 2223-105

BERESKIN & PARR

United States

**Title: METHOD AND APPARATUS FOR IMPROVED PROCESS
CONTROL IN COMBUSTION APPLICATIONS**

Inventor(s): (1) Murray J. Thomson
(2) Jason J. Nikkari
(3) Gervase I. Mackay
(4) Alak Chanda

**TITLE: METHOD AND APPARATUS FOR IMPROVED PROCESS
CONTROL IN COMBUSTION APPLICATIONS**

FIELD OF THE INVENTION

5 This invention relates to a method and apparatus for improved process control in combustion applications, and particularly those relating to the steelmaking industry.

BACKGROUND OF THE INVENTION

10 Modern steelmaking industries need to monitor the process characteristics of the steelmaking process due, in part, to the unknown composition of scrap steel that can give rise to inaccuracies in achieving the desired end point concentration of carbon and melt temperature in the final steel product. Further, real time process monitoring in the 15 steelmaking process is required to ensure safety, minimize pollutant emissions, and maximize productivity and energy efficiency—factors the steelmaking industry is sensitive to, due to increasing environmental regulations and ever greater competition within the industry.

20 Steelmaking technologies of today generally use either basic oxygen furnaces (BOFs) or electric arc furnaces (EAFs). EAFs are enjoying an increase in market share due, in part, to the EAFs ability to use 100% recycled scrap metal which, in turn, results in lower energy requirements per unit production (a large part of the energy savings for EAFs arises from avoidance of mining, smelting, and refining the raw ore). Additional 25 savings can occur since the primary energy source for EAFs is electrical energy, rather than fossil fuels—particularly desirable given that the steelmaking industry is a source of both greenhouse gases (mainly CO₂), as well as pollutants such as CO, NO_x, and other noxious substances, such as dioxins, hydrocarbons, and other particulates.

30 Notwithstanding the above benefits of EAFs current EAFs are often limited to energy efficiencies on the order of about 50–60%. Further efficiency to the steelmaking process can be achieved by improved process control during the combustion application, particularly by using

non-intrusive, real time measurements of selected off-gases and temperature produced during the combustion application. For example, reducing CO to 1-2% from current industry levels in the 10-30% range can result in substantial energy savings for large EAF operations. CO 5 provides a good empirical measure of chemical energy losses while exhaust gas temperature allows a reasonable estimate of thermal energy losses.

It can be appreciated that the requirements for a sensor to measure off-gas exhaust from an EAF is primarily driven by considerations of the 10 harsh environment that exists in the exhaust duct where the off-gas sensor is located. Exhaust temperatures can range from about 1000 K to about 2000 K. Moreover, duct gases can have high dust concentrations that can interfere with the operation of the sensor. Further, chunks of molten slag can occasionally spew up into the duct and interfere with or damage the 15 sensors.

Many commercial steel mills use extractive techniques to obtain a sample of off-gas from the exhaust. The extracted gas is cooled then analyzed using commercially available mass spectrometry or non-dispersive infrared absorption methods or chemical cells. It can be 20 appreciated, however, that the steps required to obtain a sample of the off-gas from extractive techniques can result in time delays in acquiring the data. By contrast, a process control that uses real time sensors can obtain selective measurements of the off-gas constituents and provide adjustment of the inputs to a furnace (such as oxygen, fuel, electric current, 25 etc.) on a continuous feedback loop.

Due to the harsh environment, temperature measurements are generally not available in the EAF exhaust duct because thermocouples are unable to withstand the demanding conditions.

Optical techniques, for example, can provide a non-intrusive sensor 30 for measuring real time composition of the off gas and temperature in an exhaust duct. The non-intrusive nature provides numerous operation and maintenance advantages in the harsh exhaust duct environment. Moreover, optical techniques offer the benefit of providing a line average

concentration and temperature measurement, rather than a point measurement, which can provide more accurate and reliable approximation of average conditions with an exhaust duct of a furnace. Optical techniques generally utilize a laser beam passing straight across

5 an exhaust duct.

One example of an optical based method and apparatus for off-gas composition sensing is disclosed in the United States patent, No. 5,984,998. This patent discloses transmitting a tunable diode laser with wavelengths in the mid-infrared (mid-IR) region through the off-gas

10 produced by a steelmaking furnace, and measuring the transmitted laser beam to produce a signal based on the wavelength absorption properties of the different off-gases. This measurement provides measurements of the gaseous constituents of the off-gas. Mid-IR diode lasers provide good sensitivity for certain molecules of interest in the off-gas, particularly, CO₂,

15 CO, and H₂O.

Mid-IR laser systems, however, have certain practical limitations, particularly when operating beyond the 3.0 μm wavelengths into the mid-IR range. For example, a Pb-salt diode laser operates significantly below

20 room temperature, necessitating cryogenic cooling. This adds to the complexity and cost of a steelmaking process control system.

Other problems using a mid-IR based laser diode sensor include signal saturation during high emission portions of the steelmaking process. Signal saturation can result in loss of process information during times of high emissions. Further, mid-IR light does not propagate readily

25 through available fibre optics. Accordingly, the sensor should be located near the harsh environment of the exhaust duct of the furnace. This can result in a need to design special protective equipment such as water-cooling jackets and airtight seals.

In addition, mid-IR systems use mirrors to project and align the

30 laser beam from the instrument through the desired measurement location in the exhaust duct. Ambient dust can be a problem on the electrical motors necessary to control the mirrors.

SUMMARY OF THE INVENTION

One of the most promising ways to meet competitive and regulatory pressure is through significant process control improvements. The attributes of tunable diode lasers operating in the near-infrared match very well with many of the requirements for improved process control in numerous combustion applications, including electric arc furnaces (EAFs).

The present invention provides an apparatus for process control in a combustion application, comprising a transmitting means for transmitting a near-infrared laser beam through off-gas produced by the combustion application, a detecting means for detecting the transmitted laser beam and converting the detected laser beam to an electrical signal, and a control system for providing adjustment of select inputs to the combustion application in response to the electrical signal from the detecting means.

For the purpose of this invention the wavelength of a near-infrared laser beam is in the range of about 0.7 μm to about 3.0 μm . In one embodiment the transmitting means is a tunable diode laser operating with a wavelength in the range of about 1.5 μm to about 1.7 μm . In a further embodiment of the invention the transmitting means is a distributed feedback laser operating with a wavelength in the range of about 1.57 μm to about 1.59 μm .

In a preferred embodiment of the invention the select inputs to the combustion application comprise, for example, either singly, or in combination, oxygen, fuel, and electric power—particularly where this invention is practiced on an electric arc furnace as a combustion application.

This invention also provides for a method of process control in a combustion application, comprising:

- 30 a) transmitting a near-infrared laser beam through off-gas produced by the combustion application;
- b) detecting the transmitted laser beam; and

- c) adjusting select inputs of the combustion application in response to the detected transmitted laser beam.

Moreover, the method of a preferred embodiment of this invention targets CO as one off-gas for analysis, and particularly where CO has a profile of strong lines compared to H₂O. Further, the method also targets H₂O to measure both temperature of the off-gas and H₂O concentration. While temperature measurements are necessary from a spectroscopic point of view, they are also valuable from other perspectives, including process control, quantification of exhaust gas thermal energy, improved air pollution control system design and operation, and others.

BRIEF DESCRIPTION OF THE DRAWINGS

For a better understanding of the present invention and to show more clearly how it would be carried into effect, reference will now be made, by way of example, to the accompanying drawings that show a preferred embodiment of the present invention, and in which:

- Figure 1 is a schematic view of a typical electric arc furnace;
- Figure 2 is a graph of emissions of major off-gasses from an electric arc furnace during a typical tap to tap cycle;
- Figure 3 is a schematic view of an experimental set-up;
- Figure 4 is a schematic view of a laser used in the experimental set-up of Figure 3;
- Figure 5 is a graph of the U. S. Air Force's HITRAN modelling results for H₂O at 300 K;
- Figure 6 is a graph of the U. S. Air Force's HITEMP modelling results for H₂O at 1,500 K;
- Figure 7 is a graph of the U. S. Air Force's HITRAN modelling results for CO at 300 K;
- Figure 8 is a graph of the U. S. Air Force's HITEMP modelling results for CO at 1,500 K;
- Figure 9 is a graph of the U. S. Air Force's HITEMP modelling results for CO at 2,000 K;

Figure 10 is a graph of the U. S. Air Force's HITEMP modelling results for H_2O at 2,000 K;

Figure 11 is a graph of the U. S. Air Force's HITEMP modelling results for CO_2 at 2,000 K;

5 Figure 12 is a graph of an optical response for an optimal CO line;

Figure 13 is a graph of a comparison of an isothermal CO calibration curve with test data;

Figure 14 is a graph of HITRAN modelling results for OH at 1,500 K;

10 Figure 15 is a schematic view of an optical measurement system of this invention used in an electric arc furnace;

Figure 15a is a schematic view of an alternative optical measurement system of this invention used in an electric arc furnace;

Figure 16 is a schematic view of the optical system in an exhaust duct of an electric arc furnace;

15 Figure 17 is a graph of a comparison of the gas temperature calibration curve with test data (H_2O peak height ratio versus temperature);

Figure 18 is a graph of a laser scan; and

Figure 19 is a graph of an alternative laser scan.

20 DESCRIPTION OF THE PREFERRED EMBODIMENT

Two dominant furnace technologies used in contemporary steelmaking are basic oxygen furnaces (BOFs) and electric arc furnaces (EAFs). As mentioned in the background of the invention, EAFs are enjoying an increase in market share due, in part, to the ability of EAFs to process 100% recycled scrap steel and its primary reliance on electrical energy, rather than fossil fuels, as an energy source for the combustion application. Accordingly, this invention shall be described referencing EAFs, but it is to be understood that the methods and apparatus disclosed are not to be limited to EAFs, but rather, can apply to any combustion application requiring real-time monitoring of off-gas composition and temperature, and particularly for process control.

An EAF 10 is shown in Figure 1. In general an EAF is first charged (ie., raw material is added to the furnace) with a mixture of metal (typically scrap metal) and lime. The metal is then melted (shown at 12) by creating electric arcs from the electrodes 14. The temperature around the arcs can 5 rise to 12,000°C. At this temperature a 100 tonne charge takes about 60 minutes to melt. After melting, carbon and oxygen gas are both blown or injected into the furnace at 16 and 18 to form a foamy slag layer generating and releasing large quantities of CO. The oxygen also oxidises elements in the metal, such as carbon, silicon and manganese. The acidic oxides 10 combine with the basic lime to form a neutral slag that can be poured off the surface. Carbon monoxide is also formed and escapes as a gas through exhaust duct 20. The metal is then allowed to run out of the furnace (known as tapping) into a ladle for secondary processing and casting, as needed.

15 Significant gases emitted from steelmaking furnaces such as EAFs include CO, CO₂, NO_x, H₂O, O₂, H₂, and other gases, such as hydrocarbons. The percent concentration of gas emissions from a typical EAF are shown in Figure 2, which plots extractively measured off-gas composition averaged over approximately 100 runs at a full scale EAF. It 20 can also be appreciated from Figure 2 how rapidly the conditions within an EAF can change. Variations are caused by many factors, such as, for example, charging of the EAF with scrap metal, combustion of oil and other combustible impurities, as well as injections of O₂ (blown into the furnace), CH₄, and carbon. Further, the quality of scrap steel can vary from 25 one batch to the next.

CO gives a good representation of chemical energy that is wasted when oxygen gas is blown into the furnace. H₂ emissions also provide a good representation of chemical energy not utilized effectively in the process. Figure 2 shows that CO and H₂ track each other very closely (the 30 oxygen blown into the furnace reduces both compounds concurrently releasing the chemical energy of each compound). Accordingly, so long as

one of either CO or H₂ is measured, the required information from a process control perspective is obtained.

It is also desirable to monitor temperature of the off-gas and hence obtain a measure of thermal energy losses in the combustion application.

5 As will hereinafter be detailed, this invention provides for a method of targeting H₂O to measure temperature of the off-gas.

The absorption and emission of light is related to a change in the molecular energy from one level to another, or the energy transition. In absorption, electrons are elevated to a higher energy state (describing a 10 change in rotational energy, vibrational energy, electronic energy and/or any combinations of those). and during emission this energy is discharged. The width of a typical absorption peak is less than 0.01 nm. Diode laser based optical absorption is based, in part, on conventional absorption spectroscopy, and, in particular, follows Beer's Law:

15

$$\frac{I}{I_0} = \exp[-S(T) \cdot \Phi(T,P) \cdot n \cdot L] = \exp(-A) \quad (1)$$

Where I is the laser intensity reaching the detector, I₀ is the incident laser intensity, S(T) is the temperature dependent line strength, $\Phi(T,P)$ is the temperature and pressure dependent line shape function, and takes into 20 account both temperature (Doppler) and pressure (collision) broadening mechanisms, n is the number density of the absorbing species, L is the absorption path length, and A is the absorbance.

Optical systems that offer real time analysis of the off-gas are generally based on tunable diode lasers (TDLs). In particular, with a diode 25 laser based system response times can be less than a second.

Near-infrared (near-IR) TDLs (for purposes of this invention a near-IR laser operates with wavelengths in the range of about 0.7 μ m to about 3.0 μ m) offer certain advantages for use in an optical sampling system. For example, near-IR TDLs can operate over a temperature range of about 30 0°C to about 50°C. This near room temperature operation allows lasing to be achieved using, for example, thermoelectric heating and cooling

without undue complexity or energy requirements. Moreover, the wavelengths of near-IR TDLs typically match the optical loss minima in quartz fibres, facilitating the use of fibre optic cables. Moreover, decreased sensitivity of near-IR TDLs has a benefit in that non-linear absorption can

5 be reduced (allowing Beer's Law to remain applicable for the measurement). It should be noted that decreased sensitivity of near-IR TDLs is generally not an issue in measuring the combustion of select off-gasses, such as CO, which generally need to be measured in percentages, rather than at trace levels.

10 For quantitative measurements with the best sensitivity, a laser should operate in a single mode so that only one wavelength is emitted. Near-IR TDLs have a multimode output near the lasing threshold. With increasing current applied to the laser, the output evolves to a single mode output. Near-IR lasers employing distributed feedback (DFB) are

15 constrained to single mode operation under all conditions. DFB lasers are fabricated with a miniature grating, aligned along the length of the gain region.

Single mode near-IR TDLs are suited for the detection of gases by optical absorption, or spectroscopy. The laser wavelengths coincide with

20 the absorption lines of the targeted gas molecules. Moreover, the laser wavelengths typically are less than about 50 MHz, meaning that, in general, the wavelengths are typically narrower than the pressure and temperature broadened line widths of targeted molecules. This high spectral resolution allows line specific measurements of targeted

25 species. The targeted species for industrially or environmentally significant gases from EAFs that may be measured by near-IR TDL spectroscopy include, for example, oxygen, water vapour, methane, acetylene, carbon monoxide, carbon dioxide, hydrogen halides, ammonia, hydrogen sulfide, and nitrogen oxides.

30 Near-IR TDLs are easily tunable with current and temperature, and for current designs having wavelengths below about 2.4 μm they operate at room temperature, dissipating about 100 mW of power. Moreover, DFB near-IR TDLs show continuous single mode tuning at the rate of about 0.5

cm⁻¹/°C. An additional benefit of operating in the near-IR is that pressure broadening does not present as large a problem as it does at the longer wavelengths. This is a benefit for measurements conducted at or above atmospheric pressure, as in the exhaust duct of an EAF.

5 One characteristic that limits measurement sensitivity is intensity noise or fluctuations associated with output power. The fundamental quantum limit, in the absence of any attempt to produce "squeezed light," is the shot noise associated with the detected laser power. Relative shot noise (RSN) is inversely proportional to the detected power. In addition to 10 RSN, DFB lasers produce what is referred to as relative intensity noise (RIN). RIN is expressed as the fluctuations in the detected power per unit bandwidth, divided by the detected power squared. RIN arises from amplified spontaneous emission and is inversely proportional to the cube of the detected power. At sufficiently high levels of detected power, RIN will 15 be less than the RSN, and the limit to the laser output beam will be approximately the shot noise. Typically, the intensity noise of DFB lasers is about 5 dB Hz^{-1/2} above the shot noise limit. This suggests that near-IR TDLs have best S/N ratio at high operating powers, limited only by facet damage.

20 Near-IR instruments probe overtones or combinations of the fundamental vibrational transitions. To achieve the required sensitivity a TDL can employ frequency modulation detection techniques. This can allow a TDL to measure absorbencies as small as 1 part in about 10⁵. Frequency modulation is sometimes referred to as "wavelength 25 modulation," "derivative spectroscopy," or "harmonic detection." In practice, however, frequency modulation spectroscopy and wavelength modulation spectroscopy differ only with regard to the choice of modulation frequency: frequency modulation spectroscopy involves modulation frequencies greater than the absorption line width; wavelength modulation spectroscopy involves modulation frequencies smaller than the absorption line width. Accordingly, frequency modulation spectroscopy produces distinct laser sidebands whereas wavelength modulation spectroscopy generates a continuous distribution of laser wavelengths.

Where absorption line widths exceed 1 GHz this distinction becomes important. This can occur, for example, when working with gases at atmospheric pressure or higher. Moreover, elevated temperatures increase the line widths even further due to Doppler broadening. These 5 are the type of conditions that typically exist in the exhaust duct of an EAF.

For these reasons, a preferred embodiment of this invention uses frequency modulation spectroscopy, and particularly operated at MHz frequencies; matching the modulation to the absorption line width only requires a change of the modulation amplitude. Moreover, by modulating 10 the laser frequency at MHz rates, the measurement bandwidth is shifted to higher frequencies where the laser excess noise is substantially reduced to the shot noise limit. The laser wavelength can be modulated sinusoidally by an amount comparable to the wavelength of the target optical absorption line. This modulation is readily effected by adding a 15 small AC component to the laser current. Phase sensitive electronics measure the detector photocurrent at the modulation frequency, f , or a harmonic nf . In the limit where the modulation amplitude is small compared with the spectral feature line width, the resulting demodulated signal is the n th derivative with respect to wavelength of the direct 20 transmission spectrum. Absolute absorbencies are obtained by dividing the demodulated AC signal by the detector DC output.

It is to be understood, however, that alternate sensitive techniques are possible to those skilled in the art. For example, one alternative technique is based on signal detection using a balanced ratiometric 25 detector. This technique is known to yield optical absorbencies as low as 1 ppm. With this technique, cancellation of excess laser amplitude noise is achieved by electronically balancing (rather than optically balancing) the photocurrents from each photodiode detector.

30 - EXAMPLE

From the above analysis the preferred embodiment will be described using a near-IR DFB TDL as a process sensor for use with EAFs. For a better understanding of the present invention and to show

more clearly how it would be carried into effect, the following illustrative example is provided. The example is in the form of an experiment and methodology used to select the near-IR TDL laser. Available modelling tools and research was used to assist in the selection of a promising

5 laser diode material for the wavelengths of interest to combustion applications. For example, the U. S. Air Force provides atmospheric modelling programs (known as HITRAN and HITEMP) that can be used to select an optimum wavelength region of the species of interest for combustion applications, such as CO and H₂O. In particular, HITEMP

10 modelling is available for CO, CO₂, and H₂O, whereas HITRAN modelling has a much wider selection but for complex molecules is only accurate at low temperatures. Unfortunately, current spectral databases are not well verified at the high temperatures present in combustion applications such as EAFs. Research conducted to date indicates that while models such as

15 HITEMP appear to predict line position and strength relatively well for divalent compounds such as, for example, CO, there are significant inaccuracies for triatomic compounds such as, for example, CO₂ and H₂O. It has been suggested that HITEMP is a reasonably good predictor of the high temperature absorption of water vapour: while individual line

20 positions and strengths are often erroneous, global positioning of the strongest water features is largely correct. When working in spectrally dense regions, however, even small errors in predicted position and strength can be critical.

Research and independent experimental confirmation by the

25 present inventors indicate that HITEMP predictions for CO₂ line strengths in the near-IR are very poor and appear to over predict CO₂ line strengths. The difficulty in modelling triatomic absorption lines is thought to be due to the increased number of possible energy states available to these compounds, particularly at high temperatures. Notwithstanding the

30 limitations of high temperature modelling tools, there is little alternative but to use them when selecting a laser to investigate spectral ranges.

In deciding upon the near-IR laser diode to be used in this experiment, several factors were taken into consideration, including:

- Strong spectroscopic line(s) for the species of interest, namely, CO, and H₂O, over the full range of temperature conditions (=1000–2000 K);
- Minimal interference with other species and particularly H₂O; and
- Availability/cost of the laser diode and other system components.

Once the laser is selected, the spectroscopy in the target wavelength regions are established for the range of environmental conditions to be tested. Due to the uncertainty in high temperature modelling results, particularly for H₂O, it is necessary conduct laboratory tests in order to confirm, and in some cases establish, the spectroscopy over the wavelength range and environmental conditions of interest. Once the spectroscopy is established over a representative range of test conditions, the optimal CO and H₂O absorption peaks can be selected. Accurate calibration curves over the full range of test conditions are then established using the laboratory set-up shown in Figure 3.

In the experimental set-up of Figure 3 a source of high temperature and combustion gases 22 is provided to simulate a combustible environment of an EAF and particularly the exhaust duct as at 24. A laser beam is transmitted from source 26 through fibre optic cable 28 to launch assembly 30. The laser beam is then transmitted from launch assembly 30 across region 24 to detector 32, which feeds the electronic signal back to source 26 through a coaxial cable 34. In addition, the experimental set-up features in region 24 a thin-wire thermocouple 36 to detect the temperature and an extractive analyzer 38 to measure the CO and CO₂.

To study the laser response to a wide range of high temperature target gas concentrations, a flat flame Hancken diffusion burner 40 was selected as the source of high temperature and combustion gases 22. In order to increase the measurement sensitivity, and to more accurately

represent typical path lengths present in region 24 as in full scale FAFs, a multi-pass optical absorption cell 42 was created for the lab testing. An open path Herriot type multi-pass optical set-up was used. Thermocouple 36 is a 0.020" diameter, unsheathed, type "R" (Pt-Rh) thermocouple from 5 Omega Engineering Inc. This type of thermocouple is able to withstand temperatures up to about 1723 K, and has a fast response time.

The laser source 26 used in this study is from Unisearch Associates Inc. (model number LCM-03) and is illustrated in Figure 4. This laser utilizes two-tone frequency modulation to increase the detection 10 sensitivity. The source 26 contains the DFB diode laser 44 and its temperature and current circuits, the detector 46 and its circuitry, the connector 48 to the fibre optic cable to launch assembly 30, the connector 50 for coaxial cable 34 from detector 32, the interface to the computer 52 for automatic control and data acquisition and logging, and a reference 15 cell 54 containing measurements of known concentrations of CO and CO₂.

Using a 90/10 beam splitter 56, approximately 10% of the laser beam 58 is passed to reference cell 54 to lock the laser onto the selected absorption feature. For room temperature measurements (approximately 20 0-50°C) reference cell 54 at atmospheric pressure (approximately, 100 kPa) can also serve as a secondary calibration standard. For high temperature applications, however, as, for example, found in the exhaust duct of an FAF, the calibrations found in reference cell 54 for the targeted species are inadequate. High temperature applications require calibration 25 curves to be calculated and stored, for example, in computer 52, or, for example, in a calibration cell 55. The remaining 90% of the beam is used for the measurement channel.

In particular, the laser beam is brought to one or more of the measurement locations as far as several kilometres away using a 30 standard silica fibre optic cable 28, such as those used in the telecommunication industry. This allows the controller to be placed in any suitable location within an industrial site far away from hazardous or explosive conditions in an EAF to which the launch and detector

assemblies may be exposed. To decrease connection losses and back-reflections, FC/APC fittings, such as part number F1-2069APC as supplied by Fiber Instrument Sales Inc. of New York, are used. The controller is operated by an on-board computer. The data is also directly linked to a 5 separate computer for data processing and storage via an RS-232 port provided with the controller unit.

As previously noted, while there has been a great deal of spectroscopic work done at room temperatures, much less work has been done at elevated temperatures typically found in combustion 10 applications, such as EAFs. In general, the locations and strengths of high temperature absorption features are completely independent of room temperature lines. One of the major difficulties in detecting CO and CO₂ at high temperatures is the dramatic increase in the strength and number of H₂O absorption lines compared to room temperature. For example room 15 temperature modelling results of optical absorption strengths are plotted for H₂O in Figure 5 over a range of wavelengths in the near infrared. Figure 6 shows similar results for a temperature of 1500 K—clearly showing the increase in strength and frequency of the H₂O absorption lines. Figure 7 and Figure 8 are similar to Figures 5 and 6, respectively, but for CO. Upon 20 comparing Figures 5, 6, 7, and 8, it becomes apparent that CO lines are much less frequent and generally weaker than H₂O lines. This is a limitation for CO, particularly due to the prevalence of H₂O throughout the near infrared region. Therefore it is important to select not only a strong CO region, but also one where there is minimal H₂O interference 25. However, there is uncertainty in H₂O line positions and strengths at elevated temperatures. Accordingly, the selection process involves more of a dependence on H₂O line strength and density trends, rather than exact positions. As a result, regions of relatively low H₂O absorption but strong CO lines were considered the most attractive. Figures 9, 10, and 11, show 30 HITEMP modelling of CO, H₂O, and CO₂, respectively, at 2,000 K. In particular Figure 11 shows weaker CO₂ lines in the near-IR. As mentioned

previously, research indicates even these weak predictions are much stronger than actual CO₂ absorption at elevated temperatures. Consequently, less consideration was given to choosing an optimal near-IR wavelength region based on CO₂ lines.

5 An available and affordable laser diode was then selected by looking at the several regions of equally attractive CO and H₂O absorption characteristics. The laser diode selected based on the above results can access the approximate range of 6320–6340 cm⁻¹ (1577–1582 nm).

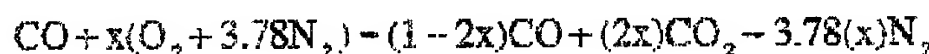
10 The first step in the laboratory tests was to compile a reference table (see Table 1) of laser current and temperature settings versus reference line locations. In combination with modelling results, this table provides a reference table to determine laser wavelengths. Once established, an approximate wavelength can be determined for each laser current and temperature setting. The location of the reference lines is 15 more or less certain due to the high degree of independent validation of room temperature features for both CO and CO₂, which are both contained in the reference cell 54.

Approximate Reference Currents (mA) for Various Diode Operating Temperatures

Temp (°C)	CD104	CD111	CD115	CD117	CD118	CD119	CD120	CD121	CD122	CD123	CD124	CD125	CD126	CD127	CD128	CD129	CD130	CD131	CD132	CD133	CD134	CD135	CD136	CD137	CD138	CD139	CD140	CD141	CD142	CD143	CD144	CD145	CD146	CD147	CD148	CD149	CD150	CD151	CD152	CD153	CD154	CD155	CD156	CD157	CD158	CD159	CD160	CD161	CD162	CD163	CD164	CD165	CD166	CD167	CD168	CD169	CD170	CD171	CD172	CD173	CD174	CD175	CD176	CD177	CD178	CD179	CD180	CD181	CD182	CD183	CD184	CD185	CD186	CD187	CD188	CD189	CD190	CD191	CD192	CD193	CD194	CD195	CD196	CD197	CD198	CD199	CD200	CD201	CD202	CD203	CD204	CD205	CD206	CD207	CD208	CD209	CD210	CD211	CD212	CD213	CD214	CD215	CD216	CD217	CD218	CD219	CD220	CD221	CD222	CD223	CD224	CD225	CD226	CD227	CD228	CD229	CD230	CD231	CD232	CD233	CD234	CD235	CD236	CD237	CD238	CD239	CD240	CD241	CD242	CD243	CD244	CD245	CD246	CD247	CD248	CD249	CD250	CD251	CD252	CD253	CD254	CD255	CD256	CD257	CD258	CD259	CD260	CD261	CD262	CD263	CD264	CD265	CD266	CD267	CD268	CD269	CD270	CD271	CD272	CD273	CD274	CD275	CD276	CD277	CD278	CD279	CD280	CD281	CD282	CD283	CD284	CD285	CD286	CD287	CD288	CD289	CD290	CD291	CD292	CD293	CD294	CD295	CD296	CD297	CD298	CD299	CD300	CD301	CD302	CD303	CD304	CD305	CD306	CD307	CD308	CD309	CD310	CD311	CD312	CD313	CD314	CD315	CD316	CD317	CD318	CD319	CD320	CD321	CD322	CD323	CD324	CD325	CD326	CD327	CD328	CD329	CD330	CD331	CD332	CD333	CD334	CD335	CD336	CD337	CD338	CD339	CD340	CD341	CD342	CD343	CD344	CD345	CD346	CD347	CD348	CD349	CD350	CD351	CD352	CD353	CD354	CD355	CD356	CD357	CD358	CD359	CD360	CD361	CD362	CD363	CD364	CD365	CD366	CD367	CD368	CD369	CD370	CD371	CD372	CD373	CD374	CD375	CD376	CD377	CD378	CD379	CD380	CD381	CD382	CD383	CD384	CD385	CD386	CD387	CD388	CD389	CD390	CD391	CD392	CD393	CD394	CD395	CD396	CD397	CD398	CD399	CD400	CD401	CD402	CD403	CD404	CD405	CD406	CD407	CD408	CD409	CD410	CD411	CD412	CD413	CD414	CD415	CD416	CD417	CD418	CD419	CD420	CD421	CD422	CD423	CD424	CD425	CD426	CD427	CD428	CD429	CD430	CD431	CD432	CD433	CD434	CD435	CD436	CD437	CD438	CD439	CD440	CD441	CD442	CD443	CD444	CD445	CD446	CD447	CD448	CD449	CD450	CD451	CD452	CD453	CD454	CD455	CD456	CD457	CD458	CD459	CD460	CD461	CD462	CD463	CD464	CD465	CD466	CD467	CD468	CD469	CD470	CD471	CD472	CD473	CD474	CD475	CD476	CD477	CD478	CD479	CD480	CD481	CD482	CD483	CD484	CD485	CD486	CD487	CD488	CD489	CD490	CD491	CD492	CD493	CD494	CD495	CD496	CD497	CD498	CD499	CD500	CD501	CD502	CD503	CD504	CD505	CD506	CD507	CD508	CD509	CD510	CD511	CD512	CD513	CD514	CD515	CD516	CD517	CD518	CD519	CD520	CD521	CD522	CD523	CD524	CD525	CD526	CD527	CD528	CD529	CD530	CD531	CD532	CD533	CD534	CD535	CD536	CD537	CD538	CD539	CD540	CD541	CD542	CD543	CD544	CD545	CD546	CD547	CD548	CD549	CD550	CD551	CD552	CD553	CD554	CD555	CD556	CD557	CD558	CD559	CD560	CD561	CD562	CD563	CD564	CD565	CD566	CD567	CD568	CD569	CD570	CD571	CD572	CD573	CD574	CD575	CD576	CD577	CD578	CD579	CD580	CD581	CD582	CD583	CD584	CD585	CD586	CD587	CD588	CD589	CD590	CD591	CD592	CD593	CD594	CD595	CD596	CD597	CD598	CD599	CD600	CD601	CD602	CD603	CD604	CD605	CD606	CD607	CD608	CD609	CD610	CD611	CD612	CD613	CD614	CD615	CD616	CD617	CD618	CD619	CD620	CD621	CD622	CD623	CD624	CD625	CD626	CD627	CD628	CD629	CD630	CD631	CD632	CD633	CD634	CD635	CD636	CD637	CD638	CD639	CD640	CD641	CD642	CD643	CD644	CD645	CD646	CD647	CD648	CD649	CD650	CD651	CD652	CD653	CD654	CD655	CD656	CD657	CD658	CD659	CD660	CD661	CD662	CD663	CD664	CD665	CD666	CD667	CD668	CD669	CD670	CD671	CD672	CD673	CD674	CD675	CD676	CD677	CD678	CD679	CD680	CD681	CD682	CD683	CD684	CD685	CD686	CD687	CD688	CD689	CD690	CD691	CD692	CD693	CD694	CD695	CD696	CD697	CD698	CD699	CD700	CD701	CD702	CD703	CD704	CD705	CD706	CD707	CD708	CD709	CD710	CD711	CD712	CD713	CD714	CD715	CD716	CD717	CD718	CD719	CD720	CD721	CD722	CD723	CD724	CD725	CD726	CD727	CD728	CD729	CD730	CD731	CD732	CD733	CD734	CD735	CD736	CD737	CD738	CD739	CD740	CD741	CD742	CD743	CD744	CD745	CD746	CD747	CD748	CD749	CD750	CD751	CD752	CD753	CD754	CD755	CD756	CD757	CD758	CD759	CD760	CD761	CD762	CD763	CD764	CD765	CD766	CD767	CD768	CD769	CD770	CD771	CD772	CD773	CD774	CD775	CD776	CD777	CD778	CD779	CD780	CD781	CD782	CD783	CD784	CD785	CD786	CD787	CD788	CD789	CD790	CD791	CD792	CD793	CD794	CD795	CD796	CD797	CD798	CD799	CD800	CD801	CD802	CD803	CD804	CD805	CD806	CD807	CD808	CD809	CD810	CD811	CD812	CD813	CD814	CD815	CD816	CD817	CD818	CD819	CD820	CD821	CD822	CD823	CD824	CD825	CD826	CD827	CD828	CD829	CD830	CD831	CD832	CD833	CD834	CD835	CD836	CD837	CD838	CD839	CD840	CD841	CD842	CD843	CD844	CD845	CD846	CD847	CD848	CD849	CD850	CD851	CD852	CD853	CD854	CD855	CD856	CD857	CD858	CD859	CD860	CD861	CD862	CD863	CD864	CD865	CD866	CD867	CD868	CD869	CD870	CD871	CD872	CD873	CD874	CD875	CD876	CD877	CD878	CD879	CD880	CD881	CD882	CD883	CD884	CD885	CD886	CD887	CD888	CD889	CD890	CD891	CD892	CD893	CD894	CD895	CD896	CD897	CD898	CD899	CD900	CD901	CD902	CD903	CD904	CD905	CD906	CD907	CD908	CD909	CD910	CD911	CD912	CD913	CD914	CD915	CD916	CD917	CD918	CD919	CD920	CD921	CD922	CD923	CD924	CD925	CD926	CD927	CD928	CD929	CD930	CD931	CD932	CD933	CD934	CD935	CD936	CD937	CD938	CD939	CD940	CD941	CD942	CD943	CD944	CD945	CD946	CD947	CD948	CD949	CD950	CD951	CD952	CD953	CD954	CD955	CD956	CD957	CD958	CD959	CD960	CD961	CD962	CD963	CD964	CD965</

To obtain reliable high temperature data the best absorption line(s) were located experimentally. Since the locations and strengths of the high temperature features are, in general, completely independent of the room 5 temperature lines that exist for the gases in the reference cell (namely, CO and CO₂), the first part of the lab work focused on finding suitable CO lines that were not significantly interfered with by water. First, the high temperature CO lines were conclusively located using pure CO as a fuel. The rich combustion of CO in air is shown below:

10



In a rich CO flame, substantial amounts of CO are present, with levels greater than 30% measured for some flame conditions. Off-gas temperatures obtained using CO as a fuel were in the range of about 1000 15 K to about 1500 K. Since CO₂ is also expected to be present in high levels for a CO flame, CO line locations were isolated from CO₂ by changing the reactant mix and observing the trends. In general, a richer flame should give off more CO than a leaner one. Once CO and CO₂ lines are differentiated, a comparison to high temperature modelling results is used 20 to verify the final CO line locations. Such validation confirms the relative accuracy of CO modelling prediction in contrast to poor accuracy of CO₂ predictions.

Having established the high temperature CO profile, a pure H₂ flame is used to obtain the high temperature water spectrum in a similar 25 manner. By combining the results of these two steps, locations of strong CO lines in combination with weak or non-existent water lines are identified.

After focusing on CO lines that are relatively removed from water lines, typical hydrocarbon fuels such as methane and propane, that 30 produce a mixture of CO, H₂O and CO₂ product gases, are used to confirm the superposition of pure CO and H₂ flame results to help find CO lines that appear to be relatively free of water interference.

It can be appreciated that certain laser settings such as the RF modulation, laser gain, and laser phase, are adjusted before any suitable CO lines are found amongst the backdrop of strong water lines. In early tests, the electronics of the laser were configured to give strong signals. 5 This had the disadvantage of resulting in relatively large line widths so that saturation was occurring for many of the strong water lines. By adjusting the laser modulation to decrease the line width, line height is sacrificed. Eventually, a point appears to be reached where the line width no longer decreases, but below which the height continues to get smaller. The 10 above procedure was conducted using the laser source 26 (from Unisearch Associates Inc., model number LCM-03). It was found that for this laser the following settings give the least possible interference, while maintaining reasonable signal strength to find as many CO lines as possible amongst the backdrop of strong water lines, namely: 15 Gain = 1700; Phase = 1550; and RF = -2.15.

The Unisearch laser uses a thermoelectric cooler temperature-stabilized near-infrared diode laser (1.58 microns) as a light source to study CO and moisture at high temperatures as, for example, would exist in electric arc furnaces. In order to correctly determine the CO 20 concentration the temperature of the furnace is monitored, and the line strength of the CO is adjusted accordingly. Moreover, if a 'clean' CO line to be monitored cannot be found at elevated temperatures (because of the presence of water lines that overlap the CO lines), the moisture level must be monitored and the CO signal corrected for the overlap with the water 25 signal.

In order to measure the furnace temperature, two appropriate water lines that vary differently in line strength with the change in temperature can be monitored. Such a measurement can provide information on the furnace temperature as well as the moisture content. Since a ST/SL mode 30 DFB lasers emit a specific wavelength of very narrow line width (compared to the line widths of the absorption signal of gases at ambient pressures and temperatures) when operated at a fixed temperature and current, the

laser requires a rapid change of its operating parameters to scan multiple lines (CO and H₂O) virtually simultaneously.

In Unisearch's laser the temperature of the laser is held constant using a thermoelectric cooler. A constant DC current is applied to the laser that brings the emitted wavelength close to the absorption line of the gas. The laser current is rapidly and repeatedly swept across the absorption feature of interest (for example, a CO absorption line) for a certain period of time (usually a few milliseconds). The laser current is then jumped to another DC setting and rapid sweeps are made at this new current setting (for example, the first H₂O line to be monitored). Another jump in DC current and rapid sweeps could scan, for example, a second H₂O line being monitored. The ramp current with such jumps and sweeps is shown in Figure 18

Since the magnitude of the modulated signal of the gas detected at 2f is proportional to the laser return power, it is important that the power be continuously monitored. The power varies from time to time due to the dust loading and the debris that crosses the laser beam. Also, the background radiation level from the arc in an electric arc furnace can be significant. A part of the background radiation from the arc that falls on the detector bandwidth is easily detected as well, along with the 'true' laser return power. This background power is be monitored and subtracted to obtain the true power to compensate for the changing magnitude of the measured signal due to dust, debris and optical misalignment. In the current configuration, the laser current is switched "OFF" as at 71 for a very short period of time at the end of each integration cycle. The background radiation that is seen by the detector is measured during this period. The laser is then switched "ON" and the scan continues.

A variation of the scan is shown in Figure 18. Here, the species 1 (CO) is scanned first (single sweep), the current is jumped to the next DC value, species 2 (H₂O - 1) is scanned (single sweep) and the current is again jumped to the next value where species 3 (H₂O - 2) is scanned (single sweep). The laser current is then switched "OFF" as at 73 and the

background radiation measured. The laser is then switched "ON" and the scan continues.

Operating the laser in a 'jump-scan' mode to monitor multiple species can be essentially simultaneous. The Unisearch laser analyzer is 5 set to make a single sweep in about 4 milliseconds. Therefore, all the three species and the background radiation can be monitored about every 15 milliseconds.

Once several attractive CO lines are located, the choices are further narrowed. In particular, closely controlled tests are conducted for various 10 air-to-fuel (A/F) ratios using propane and methane, with the lower A/F ratios resulting in increased CO production. From these tests, preliminary calibration curves can be plotted, such as that illustrated in Figure 13. Since absorption strength is a strong function of temperature for many of the lines investigated, it is important at this stage to isolate temperature 15 effects from concentration effects. The easiest way to accomplish this is to maintain a constant temperature in the flame region, for all A/F ratios. Since the A/F ratio has a significant impact on flame temperature (in addition to CO concentration), this requires using independently controlled inputs of O_2 and N_2 , rather than being limited to a fixed ratio of the two in 20 the form of air. For example, to generate increased CO in the off-gas, the oxygen/fuel ratio must be reduced to allow richer combustion. However, since the temperature will otherwise decrease when moving away from stoichiometric conditions, a concurrent reduction in the level of dilution gas (nitrogen, N_2), accomplished by a reduction in the N_2/F ratio, will allow for 25 constant temperature control.

The thermocouple cannot be in the measurement region while the optical measurements are being conducted since the laser beam path would be interrupted. Since refined temperature measurements are not critical at this stage of testing, the thermocouple is left in a fixed position 30 just above the maximum extent of the optical beam path, as confirmed with the visible alignment laser. On the basis that a fixed flow rate of reactant gases will result in an approximately constant flame plane height 25 and roughly equal convection to the thermocouple for a given fuel, the flame

plane temperature is assumed to be lower than the thermocouple measurement by a fixed amount, independent of the O_2/F ratio. In other words, it is assumed that for a fixed flow rate of influent gases, if the thermocouple temperature is the same from one O_2/F value to another, 5 then the temperature in the measurement region itself is also constant. This provides an empirical and iterative process for obtaining the influent gas settings that allow measurement of a wide range of suitable CO off-gas concentrations, with temperature held more or less constant.

To aid in the first guess at rotameter settings that result in a range 10 of CO levels over a constant temperature, adiabatic combustion is assumed to plot influent gas mixtures of various O_2/F and N_2/F levels versus adiabatic flame temperature, all of which can be predicted by software programs, such as STANJAN, and later plotted in an appropriate graphing application, such as Microsoft Excel. Levels along a particular 15 isotherm are chosen as the first iterative step and subsequent adjustments are made to these settings to obtain actual thermocouple temperatures closer to one another than the adiabatic assumption produces.

It is noted that the accuracy of the above assumptions is reduced by 20 several factors, including the assumption that flame height depends only on reactant gas flow rate and not composition, the fact that constant influent gas flow does not mean constant exhaust gas flow (due to both increased off-gas temperature and unequal moles of reactants and products), and the fact that convection is not constant due to both of the 25 above factors in addition to differences in heat capacities associated with the variable off-gas mixture.

Once the rotameter settings are determined for a given gas, the levels of exhaust gases are measured extractively using a high range detector. To save time only one measurement was obtained for each gas 30 setting regardless of how many subsequent tests were conducted for each condition. The off-gas concentrations obtained extractively are

converted from a dry basis to a wet or actual basis using the following formula:

$$\text{Actual []} = \frac{\text{Dry []}}{1 - \% \text{H}_2\text{O}} \quad (2)$$

5 Where the Dry [] represents the extractive instrument reading and the %H₂O is approximated using STANJAN (since no extractive value can be obtained).

Optical measurements are then taken for each of the promising CO lines, using the pre-set reactant gas flow rates. In this manner, curves of 10 peak height can be plotted for each of the flame conditions (and resultant CO concentrations) and the response then assessed. Using the CO concentrations obtained with the extractive probe, and corrected for water content, a plot of peak height versus CO concentration is then plotted, for example, see Figure 13.

15 An ideal response is a graded increase in CO peak height for each successively increasing extractive CO measurement. In addition, the shape of the CO line for pure CO should match that for hydrocarbon fuels such as, for example, CH₄ and propane (see Figure 12). If the width does not fit the pure CO line well at a comparable temperature, then this is an 20 indication of interference from neighbouring water lines. Further confirmation of water interference is obtained by plotting a line in the same spectral region using pure H₂ fuel. If this water line is flat or nearly flat, it can be assumed that water is not present in this region, at least for the given flame temperature. If this water line is flat and of zero magnitude, the 25 CO calibration curve for the hydrocarbon fuel will intersect zero. Finally, water interference can be assessed by confirming the independence of results for different fuels, since the combustion of fuels such as methane and propane produce significantly different amounts of water in their product gases. In general, water production is proportional to the H/C ratio 30 of the hydrocarbon fuel. Therefore, CH₄ produces a greater proportion of water than any other hydrocarbon fuel.

A good CO response for one temperature does not automatically mean the response is acceptable across the entire range of desired temperatures of about 1000 K to about 2000 K. This is due to the change in intensity of absorption lines with temperature. Therefore the above 5 procedure is repeated on a subset of CO absorption lines that were attractive at the initial temperature evaluated. This procedure can eliminate some of the CO lines that were attractive at the one temperature but would not work well across the full temperature range.

Having selected the optimal CO absorption line, the water lines are 10 then located. Selection of water lines can be an easier task than finding CO lines unaffected by water due, in part, to the frequency and strength of water absorption in this optical region. Assuming temperature is known, only one water line would be required to obtain concentration. However, the ratio of peak strengths for two water lines must be used to optically 15 obtain the temperature, since thermocouples are not suitable for EAF applications. The following should be considered in selecting the water lines:

- Strong spectroscopic line(s) for water over the full range of temperature conditions (= 1000–2000 K);
- 20 • Minimal interference with other species;
- Lines are accessible within the jump scan range of the laser; and
- Two water lines that respond differentially to changes in temperature.

25 Due to the tremendous strength and frequency already demonstrated for water lines, the first two factors are not a problem. The last point limits the range of the laser to a smaller range represented by the limits accessible by jump scanning using current alone. Jump scanning involves a limited portion of the current tuning only range. For the 30 Unisearch laser as used for this experiment, the maximum jump scan range is somewhere in the neighbourhood of 40–50 mA, representing a maximum search range of approximately 0.5 nm from the optimal CO line.

Within this range, then, the search for H_2O lines focuses on locating lines that respond differentially to changes in temperature. Optical temperature sensitivity is maximized when two lines are used from completely different absorption bands that respond in completely opposite directions to temperature, for example, optimal sensitivity can be achieved when one of the two water lines increases with increasing temperature while the other decreases. It can be appreciated, however, that both lines must be measurable over the entire temperature range.

Once two water lines are found that best meet these requirements, 10 they are used as optical temperature measurement tools. Several flame conditions (using different fuels, such as, for example, methane and propane) are tested to evaluate the change in the ratio of peak height of these two lines with changing temperature, as measured by the thermocouple.

15 After locating optimal CO and H_2O lines, increasingly accurate calibration curves are developed. Multiple regression tools (for example, the ones available in Microsoft Excel) are used to evaluate large data sets that encompass a wide range of concentration and temperature tests for each surrogate fuel. Since multiple regression can evaluate both 20 temperature and concentration effects concurrently, it is no longer necessary to confine influent gas flows by the constant off-gas temperature and flow requirements. However, it is critical to obtain representative and accurate data for each measurement. In addition, accurate calibration curves depend on a large data set.

25 The Unisearch laser of this experiment is used to record peak attributes for CO and the two water lines, such as, for example, the best of peak height, peak area, or other suitable peak attributes, as determined through statistical analysis. This data is used to optically assess temperature and concentration.

30 To assess the temperature optically for a given fuel, the ratio of the selected peak attribute for two water lines is fit against several higher order polynomials. The optimal combination of fit and minimal complexity is then used to describe the temperature-peak attribute ratio relation. An

example of a 7th order polynomial fit against peak height ratio for two water lines is given in Figure 17.

Calibration of the selected CO peak attribute as a function of temperature and concentration is accomplished in the lab via multiple regression against extractive and thermocouple data. Since H_2O concentrations are not attainable with extractive samplers, assumptions must be made to enable the correction of dry CO readings to actual CO concentrations (as per the earlier equation). In addition, the lack of independent H_2O confirmation necessitated the use of the calculated values to establish the multiple regression for H_2O peak attribute as a function of temperature and concentration. As a result of this increased uncertainty in actual H_2O concentration, the values of R^2 (a statistical measure of the error) are expected to be larger for optical determination of H_2O concentration than they are for CO concentration, since the effects of the H_2O estimate on CO concentration are limited to the amount of the correction from dry to wet concentrations.

In order to estimate the H_2O concentration, a mass balance approach using rotameter inflows is necessary, along with a consideration of the water gas shift equilibrium, which is very significant under rich conditions. The following equations were solved for CH_4 (slight modifications to the values are necessary for other hydrocarbon fuels due to the different number of carbon and hydrogen atoms) to obtain an estimate of the H_2O concentration:

$$nC = n_{CH_4} = n_T (yCO_2 + yCO) \quad \text{Equation 1}$$

$$25 \quad nO = 2 * nO_2 = n_T (2 * yO_2 + yH_2O + 2 * yCO_2 + yCO) \quad \text{Equation 2}$$

$$nH = 4 * nCH_4 = n_T (2 * yH_2 + 2 * yH_2O) \quad \text{Equation 3}$$

$$I = yN_2 + yCO + yCO_2 + yH_2 + yH_2O + yO_2 \quad \text{Equation 4}$$

$$N_2 = n_T * yN_2 \quad \text{Equation 5}$$

$$CO_{(g)} + H_2O_{(g)} \rightleftharpoons CO_{2(g)} + H_{2(g)} \quad \text{Equation 6}$$

$$30 \quad K_p = \exp[\Delta G^\circ_T / (R_n T)] \quad \text{Equation 6a}$$

$$\Delta G^0_T = \sum v_i g^0_{i,T}$$

Equation 6b

$$y_{CO} = X_{CO} (1 - y_{H_2O})$$

Equation 7

Where:

n_X = molar inflow of reactant gas X through the rotameters

5 (obtained from rotameter calibration chart) [moles]

y_X = mole fraction of product gas X in the off gas

n_T = total product gas (exhaust) flow [moles]

K_p = equilibrium constant

ΔG^0_T = standard Gibb's function change [J]

10 R_u = universal gas constant [8.314 J/(mol·K)]

T = temperature [K]

v_i = moles of component "i" from balance chemical equation

$g^0_{f,T}$ = Gibb's function of formation [J/mol]

X_{CO} = Dry concentration of CO (extractive reading)

15 Dilution from the shroud flow (N_2) into the combustion region were considered using an iterative approach based on "Equation 1." Wherever CO and CO_2 extractive data are available (i.e., not off scale for the extractive device), any apparent deficiency between the inflow of C moles (from the fuel) and the outflow in the form of CO and CO_2 is caused by some shroud nitrogen penetrating to the extractive measurement location. Quantification of this dilution and correction of the predicted concentrations allows increasingly accurate predictions to be made.

20 To further improve temperature and extractive sampling accuracy the thermocouple and sample probe measurements are conducted at the same point where optical measurements are obtained. While significant variation in temperature and concentration is expected in the measurement region, single measurements in the middle of the measurement region are used to obtain "average" values. Ideally, multiple measurements are taken throughout the region to obtain an even more representative temperature and concentration profile. Since the thermocouple and extractive probe will block the laser beam when placed

in the measurement region, an accurate and repeatable method must be used to move the thermocouple and probe into the same position each time measurements are taken. To accomplish this the probe and thermocouple were attached at the same position to a vertical kinematic 5 stage to ensure reproducibility of the measurement location. One temperature and extractive measurement is taken either before or after each optical test.

Optical results for the most attractive CO line in the measurement region accessible by this laser are shown in Figure 12. These 10 measurements were obtained using methane as a fuel with thermocouple temperatures of about 1550 K. Pure CO was also used as a fuel for comparison purposes. Several things worth noting include the exact matching of the methane profile with the pure CO flame width to the left of the peak. To the right of the peak there is some difference due to 15 superposition with the tail of a small H₂O peak (the left side of the peak is somewhat visible at the right edge of the graph). This indicates minimal interference with water.

By using experimental absorption measurements over a wide range of representative gas conditions it was determined that the CO 20 absorption line located at 1577.96 nm was the optimal CO feature present within the 1577–1582 nm operating range of the selected laser. The optimal water absorption lines were 1577.8 nm and 1578.1 nm. Figure 12 shows increasing absorption peak height with increasing CO concentration under roughly isothermal test conditions.

25 An analysis of the method's accuracy has been conducted using 209 calibration and 105 unique test burner setpoints. The burner setpoints had a random distribution across CO concentration (from 0 to 10%) and gas temperature (from 970 to 1480°C). The water concentration varied from 3 to 27%. The calibration data set and multiple regression analysis 30 provided calibration curves linking the absorption peak heights with measured gas concentrations and temperatures. The test data set was used to independently evaluate accuracy. It was found that peak height gave a slightly better correlation with CO concentration than did peak area.

The CO concentration increased linearly with CO peak height. There was a weak dependence on temperature. A small correction for the water concentration was required. The multiple regression analysis provided a calibration curve of CO concentration as a function of the CO and water peak heights. The correlation had an R squared of 0.96, indicating excellent representation of the data

Figure 13 compares the CO peak height to the measured CO concentration for groups of data that had temperatures within a $\pm 20^{\circ}\text{C}$ range. The isothermal calibration curves are also shown. These results show that the CO peak height response is essentially linear with CO concentration, with a slight offset attributed to a weakly interfering water absorption line nearby. An error analysis using the previously established calibration curve and the test data indicates that this optical technique is able to measure CO concentrations within a standard deviation of 0.47% CO. This value is comparable to the accuracy of extractive systems and is considered to be satisfactory in light of the high CO concentrations present in many EAFs, where levels in excess of 20% CO are common.

The gas temperature increased linearly with the ratio of the water peak heights. The multiple regression analysis determined a calibration curve with an R squared of 0.92. Figure 6 shows the variation of the selected water peak height ratio with temperature. The test data analysis found a standard deviation of the error of 36°C . The use of two separate lasers to access more widely separated water lines is likely to improve temperature measurement sensitivity considerably.

There were numerous difficulties pertaining to the measurement of CO_2 at the desired temperatures. Unlike CO, the absorption peaks were very weak at elevated temperatures for this gas in most areas of near-IR, including a specific region selected. Combined with the increase in H_2O peak strength and intensity, this made CO_2 measurements difficult in the initial test range. Using HITFMP modelling results, it became apparent that an alternate region in the near-IR contained some strong CO_2 lines that appeared to be sufficiently far away from neighbouring H_2O lines for

temperatures from about 1000 K to about 2000 K. A more promising region for high temperature CO₂ measurements is around 2.0 μm .

It was discovered during this experiment that two particularly strong OH absorption lines were readily accessible within the jump scan range of 5 the selected CO peak. The approximate locations of these two lines were confirmed by HITRAN modelling results, as shown for 1500 K in Figure 14. While these two lines are very close together, it is not possible to use their ratio for temperature determination. One reason is that they appear to move very much in sync over a wide range of temperatures.

10

- APPLICATION TO AN ELECTRIC ARC FURNACE

A schematic of an EAF system using the process sensor of this application is shown in Figure 15. A more detailed view of the exhaust duct is shown in Figure 16. In general Figure 15 shows an EAF 10 having an 15 exhaust duct 20. A laser source 26 is provided to transmit a laser beam through fibre optic cable 28 to a launcher assembly 30 (see Figure 16). The laser beam is transmitted across duct 20 as at 60 to detector 32 which, in turn, transmits an appropriate electronic signal back to source 26 via a coaxial cable 34. It can be appreciated that a fiber optic cable can 20 also be used in place of coaxial cable 34. Source 26, through use of a computer that can be located on-board (for example, see Figure 4) uses the calibration curves calculated for high temperature applications to interpret the readings of the concentration of, for example, CO, from detector 32 and sends an appropriate signal to an EAF process control 25 system 62. Control system 62 can then adjust the oxygen flow through controller 64, or temperature of the EAF through, for example, natural gas flow controller 66, as needed. As illustrated Figure 15 illustrates a process control system that uses a real time sensors to obtain selective measurements of the off-gas constituents and provides adjustment of the 30 inputs to a furnace (such as oxygen, fuel, electric power, etc.) on a continuous feedback loop.

Although the laser beam propagates through the measurement path 60 in the exhaust duct 20, small holes 68 and 70 in the duct allow the

laser launch assembly 30 and detector 32, respectively, to be located away from the harsh conditions within the exhaust duct. Accuracy concerns can arise, however, due to the in-leakage of room air through the small holes 68 and 70. It is expected that the contribution of ambient gases to 5 the measured signal strength should be negligible, however. This is principally related to the fact that the high temperature optical absorption wavelengths selected have no significant room temperature absorption for species likely to be present in the steel plant ambient air, according to HITRAN modelling results. Moreover, any dilution of stack gases by the 10 relatively small inflow of ambient air can be further minimized by designing the optical interface in such a manner that ambient air is largely directed at an angle downstream into the stack beyond the measurement zone.

A schematic of an EAF system using an alternative process of this invention is shown in Figure 15a. Except where noted and described 15 below the same reference characters will be used to identify the same parts in both figures. In Figure 15a the launcher assembly 30' transmits the laser beam across a gap 74 between duct 20 and exhaust duct 76. The laser beam is detected by detector 32' which, in turn, transmits an appropriate electronic signal back to source 26 via cable 34. Such an 20 arrangement enables the launcher assembly and detector to be placed away from duct 20 and the high temperature environment of the off-gas. Accuracy concerns are minimized due to the relatively small size of the gap compared to the large diameters of the ducts 20 and 76.

With slightly different laser diodes that still operate in the near-IR, 25 absorption models and limited research indicate the potential to measure CO₂, NO, hydrocarbons, HX (where X represents various halogens), and H₂S compounds. By multiplexing additional lasers through a shared optical system (optical launch and receive components, fibre optic transmission cables, laser electronic control components, etc.) the 30 incremental system cost for this measurement capability may be a small fraction of the total system cost since the laser diodes themselves typically represent a small fraction of the total system capital cost. This possibility

would extend the benefits of near-IR optical measurement techniques to an extremely wide range of applications.

Moreover, visible lasers offer many of the same advantages of near-IR lasers, including, for example, cost, simple operation, and efficient 5 transmission through conventional fibre optics. Attractive regions for O₂ detection lie in the visible wavelengths, especially around 0.76 μ m. NO₂ detection in the visible wavelengths has been documented around 0.68 μ m.

While this technique has been investigated specifically for 10 application in the steel industry, and more specifically for EAFs, there exists tremendous potential for extension to near-IR measurement of additional compounds and application to numerous other combustion devices. Some particular examples can include: steel production (smelting, reheat furnaces, BOFs, etc.); aluminum smelters and other 15 metallurgical applications; potash processing; fossil fuelled power generation plants; incineration; glass furnaces; cement kilns; and recovery boilers in the pulp and paper industry.

It can be appreciated that variations to this invention would be readily apparent to those skilled in the art, and this invention is intended to 20 include those alternatives.